https://doi.org/10.5194/essd-2020-340
Preprint. Discussion started: 15 January 2021

Open Access Earth System Science Data Discussions

A 14-yr Circum-Antarctic Iceberg Calving Dataset Derived from Continuous Satellite Observations

Mengzhen Qi[1,3,5*], Yan Liu[1,3,5*], Jiping Liu[4], Xiao Cheng[2,3,5†], Qiyang Feng[1], Qiang Shen[6,7], Zhitong Yu[8]

[1] State Key Laboratory of Remote Sensing Science, and College of Global Change and Earth System Science, Beijing Normal University, Beijing 100875, China
[2] School of Geospatial Engineering and Science, Sun Yat-Sen University, Zhuhai 519082, China
[3] Southern Marine Science and Engineering Guangdong Laboratory, Zhuhai 519082, China
[4] Department of Atmospheric and Environmental Sciences, University at Albany, State University of New York, Albany, NY 12222, USA
[5] University Corporation for Polar Research, Beijing 100875, China
[6] State Key Laboratory of Geodesy and Earth's Dynamics, Innovation Academy for Precision Measurement Science and Technology, Chinese Academy of Sciences, Wuhan 430077, China
[7] University of Chinese Academy of Sciences, Beijing 100049, China
[8] China Academy of Space Technology, Qian Xuesen Laboratory, Beijing 100094, China

*These authors contributed equally to this work.

† *Correspondence to*: Xiao Cheng (chengxiao9@mail.sysu.edu.cn)

Abstract. Iceberg calving is the main process that facilitates the dynamic mass loss of ice sheets into the ocean, which accounts for approximately half of the net mass loss of all Antarctic ice shelves. Fine-scale calving variability observations can help reveal the involved calving mechanisms and identify the principal processes that influence how the changing climate affects the mass loss of ice sheets. Iceberg calving from specific ice shelves or regions has been monitored before, but there is still a lack of consistent, long-term and high-precision records on independent calving events for all Antarctic ice shelves. In this study, we developed a circum-Antarctic annual iceberg calving product measuring every independent calving event larger than 1 km^2 that occurred from August 2005 to August 2019. We first simulated the expansion of the coastline according to ice velocity, and then manually delineated the calved areas, which are considered to be the differences between the simulated coastline and the actual coastline derived from the corresponding satellite imagery, based on 15 years of continuous multisource optical and synthetic aperture radar images. This product provides detailed information on each calving event, including the associated year of occurrence, area, size, average thickness, mass, recurrence interval, type, and measurement uncertainties. In total, 1786 annual calving events occurred on the Antarctic ice shelves from August 2005 to August 2019. The average annual calving area was measured as 3411.4 km² with an uncertainty value of 17.1 km², and the average calving rate was measured as 771.1 Gt/yr with an uncertainty value of 10.2 Gt/yr. The calving frequency, area, and mass fluctuated moderately during the first decade, followed by a dramatic increase from 2015/16 to 2018/19. During the dataset period, large ice shelves, such as the Ronne-Filchner, Ross and Amery Ice Shelves, advanced with low calving frequency, while small and medium-sized ice shelves retreated and calved more frequently. Iceberg calving is most prevalent in West Antarctica, followed by the Antarctic Peninsula and Wilkes Land in East Antarctica. The annual circum-Antarctic iceberg calving dataset provides

https://doi.org/10.5194/essd-2020-340
Preprint. Discussion started: 15 January 2021

consistent and precise calving observations with the longest time coverage. The dataset provides multidimensional variables for each independent calving event that can be used to study detailed spatiotemporal variations in Antarctic iceberg calving. The dataset can also be used to study ice sheet mass balance, calving mechanisms and the responses of iceberg calving to climate change. The dataset is shared via Global Change Data Repository (http://www.geodoi.ac.cn/WebEn/doi.aspx?Id=1516), and entitled "Annual iceberg calving dataset of the Antarctic ice shelves (2005-2019)" with DOI: 10.3974/geodb.2020.04.09.V1

1 Introduction

The ice shelves surrounding Antarctica's coastline play an important role in the stability of the Antarctic ice sheet and its mass balance. Iceberg calving is a process whereby the ice from a glacier or ice-shelf frontal edge is stripped away and enters the ocean. Iceberg calving accounts for approximately half of the net mass loss of all Antarctic ice shelves (Depoorter et al., 2013;Rignot et al., 2013a). Enhanced iceberg calving can indirectly lead to ice shelf instability, which accelerates the outflow of tributary glaciers into the ocean, causing sea level rise (Berthier et al., 2012;Furst et al., 2016;Rignot et al., 2004). In-depth studies of the calving process are essential to accurately predict the impact of future climate change on ice shelves/sheets and sea levels.

Model simulations and remote sensing observations are two major tools used to study iceberg calving. The former focus on simulating the dynamic process of a calving front in response to atmospheric and oceanic forcings and stress within ice sheets. Different models are used to understand the evolution and changes of ice shelves (Hill et al., 2018;Lovell et al., 2017;Luckman et al., 2015;Miles et al., 2017). The latter focus on the monitoring and quantitative assessment of calved areas using remotely sensed data, which can be assimilated into ice sheet models to further improve the accuracy of model simulations (Massom et al., 2018;Pattyn and Morlighem, 2020).

Research on remotely sensed iceberg calving monitoring can be classified as having three main focuses: (1) observations of specific ice shelves or glaciers with high spatial resolution data, e.g., long-term monitoring of the Pine Island Glacier, Mertz Glacier Tongue, and Amery Ice Shelf (Bindschadler, 2002;Massom et al., 2015;Zhao et al., 2014); (2) observations made of larger regions with lower spatial and temporal resolution data, e.g., calving monitoring along the Antarctic Peninsula and Ross Sea coast (Cook et al., 2005;Cook and Vaughan, 2010;Fountain et al., 2017); and (3) circum-Antarctic calving front observations of specific years based on satellite image mosaics of the Antarctic coastline (Liu and Jezek, 2004;Liu et al., 2015;Scambos et al., 2007;Yu et al., 2019). The first two types of studies achieve the precise monitoring of calving events in specific ice shelves or small areas while the third type quantitatively assesses iceberg calving at the continental scale. Liu et al. (2015) extracted 579 independent calving events for six years from the Envisat ASAR circum-Antarctic mosaic. The authors obtained comprehensive, detailed iceberg calving observations at different scales through image matching and feature tracking, which made it possible to investigate calving patterns and mechanisms. Their work laid the foundation for the subsequent exploration of the physical triggers of small and large calving events (Medrzycka et al., 2016) and revealed the "self-organized critical systems" of glaciers and ice sheets at different calving scales (Åström et al., 2014).

https://doi.org/10.5194/essd-2020-340
Preprint. Discussion started: 15 January 2021


Open Access Earth System Science Data Discussions

The long-term and high-precision remote sensing observation of circum-Antarctic independent calving events not only describes the spatial and temporal features of iceberg calving but also provides fundamental data for further investigating calving mechanisms and estimating ice-shelf mass balance in response to climate change. In this study, we identify annual calving events through a combination of a velocity-based ice shelf front edge simulation and semiautomatic annual iceberg calving extraction. We further acquire the calved-area outline, location, year of occurrence, area, thickness, mass, recurrence interval, and type of each calving event. Building on this, we develop a circum-Antarctic iceberg calving dataset. The dataset spans August 2005 to August 2019. Using this product, we analyse the spatial and temporal characteristics of iceberg calving for the last 14 years.

2 Data

2.1 Satellite imagery

Considering the relatively low calving frequencies measured in August of each year (Liu et al., 2013) and the time limitations of available satellite images, we define the annual calving recurrence interval as running from August of the current year to August of the following year. We know that it is difficult to create such a circum-Antarctic iceberg calving dataset based on a single satellite platform. To continuously monitor Antarctic iceberg calving for 2005 to 2019, multisource remotely sensed data are used in this study. We prioritize using SAR (Synthetic Aperture Radar) images for early August each year given that their quality is minimally affected by polar nights and cloudy days. For periods and areas for which SAR data are not available, optical images for close dates are used instead. Satellite images used in the development of this product include Wide Swath Mode (WSM) images from ENVISAT (Environmental Satellite) ASAR (Advanced Synthetic Aperture Radar) for 2005 to 2011 (downloaded from http://eogrid.esrin.esa.int/browse), MODIS (Moderate-resolution Imaging Spectroradiometer) 250 m Calibrated Radiances Product images (MCST, 2017) for 2012 to 2014 (downloaded from https://worldview.earthdata.nasa.gov/), the synthetic images of Landsat-8 OLI (Operational Land Imager) for bands 4 (630-680 nm), 3 (525-600 nm), and 2 (450-515 nm) for 2013 to 2019 (downloaded from https://www.usgs.gov/), and the Extra Wide Swath (EW) mode images of Sentinel-1 SAR for 2015 to 2019 (downloaded from https://www.esa.int/ESA). Detailed descriptions of these data are given in Table 1.

2.2 Supplementary datasets

Additional remote sensing data were also used to facilitate product development and analyses. MEaSURE InSAR (interferometric synthetic aperture radar)-based Antarctica ice velocity map version 2 (Rignot et al., 2011;Mouginot et al., 2012) is used to simulate the expansion of the ice-shelf frontal edge and locate calved areas. MEaSUREs Antarctic Boundaries Version 2 (Rignot et al., 2013b) is used for the ice shelf delineation and spatial analysis of the calving distribution. Two ice thickness datasets (Bedmap 2 and Bedmachine) (Morlighem et al., 2020;Fretwell et al., 2012) are used for calving thickness extraction and mass calculation. The Reference Elevation Model for Antarctica (REMA) (Howat et al., 2019) is used for the uncertainty evaluation of the extracted thickness. The Antarctic daily surface melt dataset (Picard and Fily, 2006) is used to

https://doi.org/10.5194/essd-2020-340
Preprint. Discussion started: 15 January 2021

analyse the response of iceberg calving to ice sheet surface melting. Detailed descriptions of each remote sensing product used are presented in Table 2.

Table 1: List of satellite images used in the development of a circum-Antarctic iceberg calving product for 2005-2019

Satellite	Sensor	Product level	Agency	Swath	Revisit period in polar regions	Spatial resolution	Number of Images	Time range	Data acquisition
ENVISAT	ASAR (WSM)	L1B	ESA	405 km	Less than 10 days	75 ×75 m	5046	2005/08 - 2012/04	http://eogrid.esrin.esa.int/browse
Sentinel-1	SAR (EW)	L1 GRD	ESA	400 km	Less than 6 days	20×40 m	3780	2015/01 - 2020/01	https://www.esa.int/ESA
Terra/Aqua	MODIS	L1B	NASA	2330 km	1-2 days	250×250 m	168	2012/01 - 2014/12	https://worldview.earthdata.nasa.gov/
Landsat-8	OLI	L1GT	NASA	190 km	Less than 16 days	30 ×30 m	15674	2013/11 - 2019/12	https://www.usgs.gov/

Table 2: List of other remote sensing products used in the development of a circum-Antarctic iceberg calving product for 2005-2019

Dataset	Measurement methods (in ice-shelf areas)	Temporal coverage	Accuracy	Data Format	Agency	Data acquisition	Reference
MEaSUREs InSAR-Based Antarctica Ice Velocity Map Version 2	InSAR	1996-2016	1-17 m/yr	450×450 m raster	NSIDC	https://nsidc.org/data/NSIDC-0484/versions/2	(Rignot et al., 2017)
MEaSUREs Antarctic Boundaries Version 2	DInSAR	1992-2015	25-250 m	Vector	NSIDC	https://nsidc.org/data/nsidc-0709/versions/2	(Rignot et al., 2013b)
Bedmachine	Hydrostatic equilibrium	1970-2019	10 m	500×500 m raster	NSIDC	https://nsidc.org/data/nsidc-0756	(Morlighem et al., 2020)
Bedmap 2	Satellite radar and laser altimetry, hydrostatic equilibrium	1970-2000	~100 m, bias -13-53 m	1×1 km raster	BAS	https://secure.antarctica.ac.uk/data/bedmap2/	(Fretwell et al., 2012)
The Reference Elevation Model for Antarctica (REMA)	Stereo photogrammetry	5/9/2015 ± 432 days	Less than 1 m	Digital Elevation Model	PGC	https://www.pgc.umn.edu/data/rema/	(Howat et al., 2019)

https://doi.org/10.5194/essd-2020-340
Preprint. Discussion started: 15 January 2021

Dataset of daily surface melt in Antarctica	Passive microwave radiometer (SMMR and SSM/I)	1979-2018	—	25×25 km raster	UGA	http://pp.ige-grenoble.fr/pagesperso/picardgh/melting/	(Picard and Fily, 2006)

* Abbreviations. NSIDC for National Snow and Ice Data Center, BAS for British Antarctic Survey, PGC for Polar Geospatial Center at University of Minnesota and UGA for Université Grenoble Alpes.

3. Method

An annual calving event occurs when an independent calved area has an outline that does not overlap or is spatially adjacent to other calving events occurring in the same year (even if it occurs on the same ice shelf), namely, the topology requires nonoverlapping and nonadjacent annual calved-area polygons for the specific year. Data generation involves the following three steps: preprocessing the data, extracting iceberg calving, and acquiring attributes (Figure 1). Each of these steps is discussed in the following sections. In addition, the consistency of multisource satellite imagery used in monitoring annual iceberg calving has been validated.

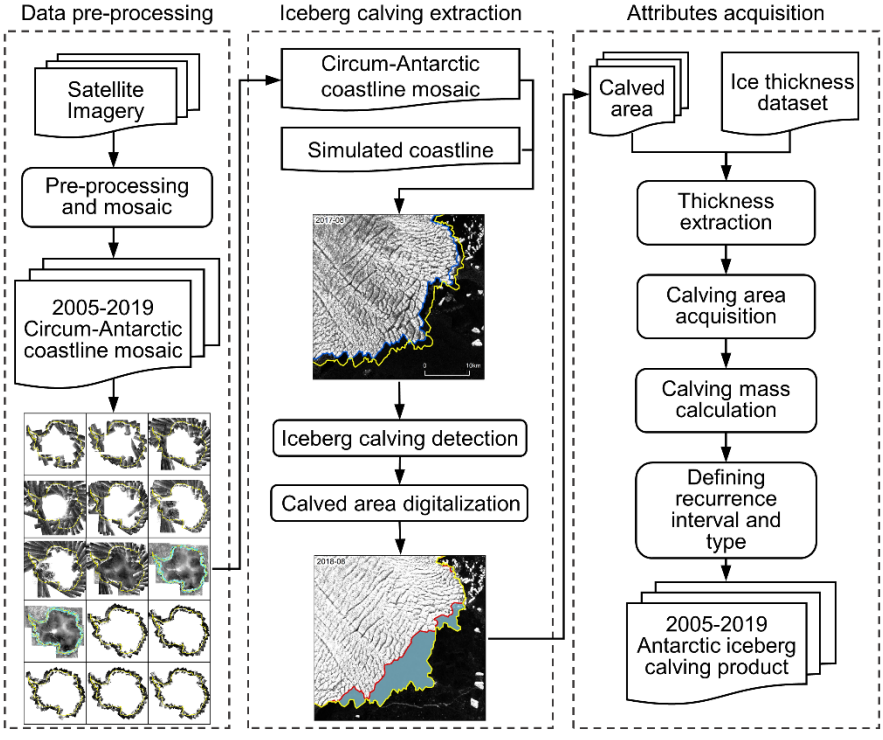

Figure 1: Outline of our methodology. Satellite images are preprocessed to obtain the annual mosaic of the Antarctic coastline. Based on the circum-Antarctic coastline mosaic and corresponding simulated coastline, we extracted calved areas. Then, we acquired attributes such as thickness, area, mass, recurrence interval, and type to produce an annual iceberg calving product for the Antarctic ice shelves.

3.1 Data preprocessing

Data preprocessing involves geocoding, geometric correction, and mosaic generation. SAR images for the first three days of each month of August are used preferentially to generate the circum-Antarctic coastline mosaic for the periods of 2005-

https://doi.org/10.5194/essd-2020-340
Preprint. Discussion started: 15 January 2021

2011 and 2015-2019. For 2012-2014, data vacancies were filled with images of the same sensors from close dates. For the mosaic for 2012, we used MODIS images for September combined with SAR images for April to facilitate detection. For 2013 and 2014 without SAR images, we chose both MODIS and Landsat-8 OLI circum-Antarctic coastline mosaics to extract iceberg calving. To reduce errors due to different imaging times, we overlaid the satellite image strictly by time ordering, namely, images taken on a date closer to 1st August should be on the upper layer. The preprocessing results of the remotely sensed data are shown in Figure 2, which provide good coverage of the Antarctic coastline and the frontal edges of ice shelves.

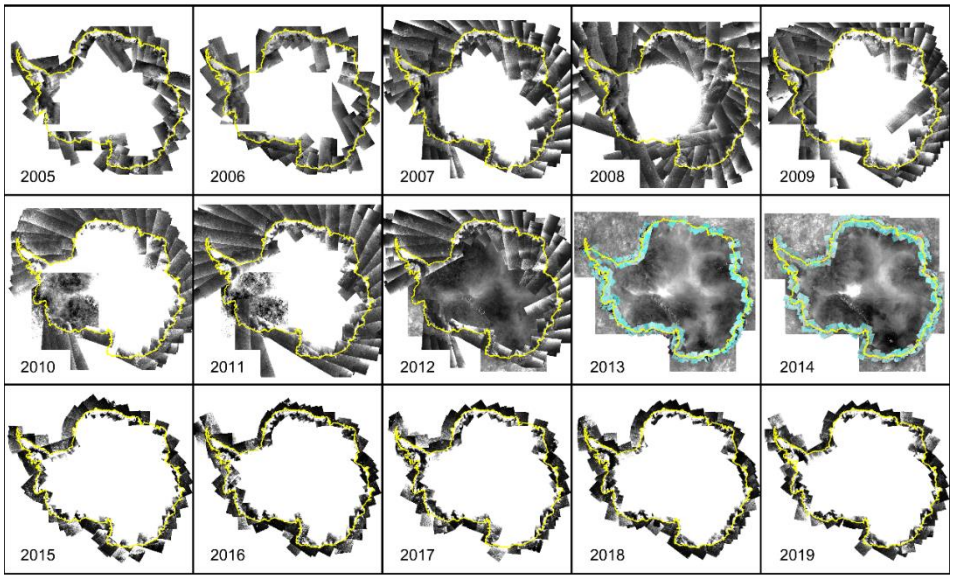

Figure 2: Schematic showing the results of satellite imagery preprocessing. We used Envisat ASAR images for 2005-2012, Landsat-8 OLI images for 2013-2014, MODIS images for 2012-2014, and Sentinel-1 SAR images for 2015-2019.

3.2 Iceberg calving extraction

To create the annual iceberg calving dataset for the Antarctic ice shelves, we simulated the expansion of the ice-shelf frontal edge and detected the calved areas based on satellite images. We first manually digitalized the coastline in August 2005, 2010, and 2015 as the input benchmark coastline. Then, the following steps were iterated for the extraction of every annual calving cycle with the methodology divided into two overarching tasks: velocity-based ice shelf front edge simulation and semiautomatic annual iceberg calving extraction (Qi et al., 2020).

a) Velocity-based ice shelf front edge simulation. We converted the vertices of the input coastline to obtain the set of coastline feature points for a specific year. Based on the velocity at the position of each coastline point, we calculated the movement of feature points over the duration of the given year. By lining up the moved feature points sequentially, a new coastline was derived, namely, the simulated coastline of the next year, as shown with yellow lines in Figure 3.

Additionally, we conducted a controlled experiment on the impact of different ice velocity products while simulating the next-year coastline. Fifty points on the high-flowing Pine Island Glacier were randomly selected as samples. We simulate their 11-year movement using both the average ice velocity map (Rignot et al., 2017) and MEaSUREs Annual Antarctic Ice Velocity

https://doi.org/10.5194/essd-2020-340
Preprint. Discussion started: 15 January 2021


Open Access Earth System Science Data Discussions

Maps for 2005-2017 (Mouginot et al., 2017). The results show that over the 11 years, the cumulative error between points moved under different ice velocity products by 0.15 km to 14.45 km with an average value of 3.96 km and a standard deviation of 4.09 km. We assume that errors introduced by using the average ice velocity map to simulate the ice-shelf frontal edge of different years are acceptable.

For the non-calving area, theoretically, the simulated coastline should fit the real coastline shown in a remotely sensed image well, but due to the geographical bias of images and errors of the ice velocity product, some deviations between the directly obtained simulated coastline and actual coastline may occur. Therefore, before extraction, we first checked and rectified the simulated coastline to ensure that it fit the actual coastline in non-calving areas. After manual correction, the extraction results were found to be of good accuracy.

b) Iceberg calving extraction. We manually rectified the simulated coastline to ensure that after rectifying, it fit the real coastline shown in the corresponding satellite images. Then, we obtained the actual coastline for the next year, which is shown as the red line in Figure 3. We extracted the enclosed area between the simulated coastline and actual coastline to acquire the calved area (the blue area in Figure 3). After extracting for one annual calving cycle, we checked topological relations at the continental scale for this year. We ensured that calved-area polygons did not intersect with each other and then obtained vectors for each calved area for the given year.

This iceberg calving extraction method employs a simple process and broad applications. The actual coastline modified from last year's extraction can be used as the input coastline of the next year's extraction; thus, we can provide time-continuous iceberg calving monitoring and effectively avoid repetition and omission errors. Additionally, semiautomatic operation offers incomparable precision and efficiency, greatly reducing the postprocessing workload.

https://doi.org/10.5194/essd-2020-340
Preprint. Discussion started: 15 January 2021

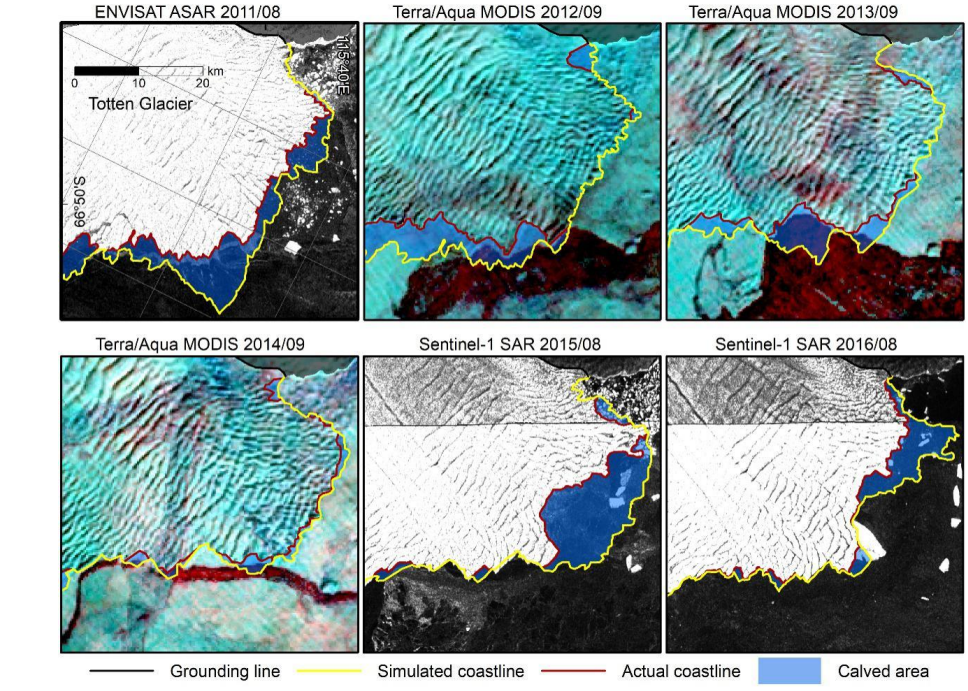

Figure 3: Schematic of the calved area extraction method displaying different sources of satellite imagery used for annual iceberg calving extraction for 2011 to 2016. Red lines represent the actual coastlines. Yellow lines represent the simulated coastlines. Blue areas represent the extracted calved areas.

3.3 Attribute acquisition

For individual calving events, attributes include the area, calving scale, average thickness, mass, calving recurrence interval, type, and uncertainties of relevant parameters. Therefore, the acquisition of calving areas and masses, uncertainties, recurrence intervals and their classifications are discussed in the following sections.

3.3.1 Calving area and mass

After acquiring vectors of the calved area polygons, we calculated their areas under polar projection. Then, these values were divided into four different scales: small-scale (< 10 km^2), medium-scale (10-100 km^2), large-scale (100-1000 km^2), and extra-large-scale values (>1000 km^2). We further obtained the average thickness of each calved area from the Antarctic ice thickness products (Bedmap 2 and Bedmachine). Based on area and thickness, the calving mass (C) was calculated from Eq. (1):

$$C = A_c \times \overline{H} \times \rho_{ice}, \quad (1)$$

where A_c stands for the calving area and $\overline{H}$ represents the average thickness of the calved area. The standard value of ice density $\rho_{ice} = 917\ kg/m^3$ was used for the calculation.

https://doi.org/10.5194/essd-2020-340
Preprint. Discussion started: 15 January 2021


Open Access Earth System Science Data Discussions

180 **3.3.2 Uncertainty assessment**

The uncertainties involved in the calculation of calving mass based on Eq. (1) include errors of calving area measurement, thickness extraction, and ice density. The uncertainty of the calving area is determined by the accuracy of the extraction method. Thickness uncertainty should be theoretically affected by top surface elevation measurements and firn depth correction; in reality, there are also uncertainties in thickness changes with time, according to hydrostatic equilibrium assumptions, and in
185 the offsets in locations during extraction. In this section, we evaluate the main uncertainties encountered during the development of the annual iceberg calving dataset.

a) Calving area uncertainty. Calving area uncertainty is mainly determined by the spatial location biases of calved-area outlines, which are related to both the original image resolution and the perimeter of the calved area. The equivalent perimeter width extracted by this method based on 75 m resolution images is 0.005 km (Qi et al., 2020); therefore, the uncertainty of the
190 calving area (U_A) can be calculated from Eq. (2):

$$U_A = 0.005 \times l, \tag{2}$$

where l represents the perimeter of each calving event (km).

b) Thickness uncertainty. The ice-shelf thickness dataset used in this product is derived from the hydrostatic equilibrium (Morlighem et al., 2020), which is written as Eq. (3):

195 $$H = (s - \delta)\frac{\rho_w}{\rho_w - \rho_{ice}} + \delta, \tag{3}$$

where H denotes ice-shelf thickness. s is the top surface elevation, namely, the height of the snow top. δ is firn depth correction, and $\rho_w = 1027\ kg/m^3$ is the density of seawater.

Therefore, thickness uncertainty ($U_{\overline{H}}$) can be evaluated from Eq. (4):

$$U_{\overline{H}} = \overline{H} \times \sqrt{\frac{U_{s_c}^2}{s_c^2} + \frac{U_\delta^2}{\delta^2} + \frac{U_{\rho_{ice}}^2}{\rho_{ice}^2} + \frac{U_{\rho_w}^2}{\rho_w^2}}, \tag{4}$$

200 where $\overline{H}$ and s_c represent the average thickness and average surface elevation of the calved area, respectively. U_{s_c} is the uncertainty of the calved-area surface elevation, U_δ is the uncertainty of firn depth correction, and $U_{\rho_{ice}}$ and U_{ρ_w} represent the uncertainty of ice and seawater density, respectively.

For the calculations, 917 kg/m^3 is used for ρ_{ice} and 1027 kg/m^3 is used for ρ_w, and their uncertainties $U_{\rho_{ice}}$ and U_{ρ_w} are valued at 5 kg/m^3 (Griggs et al., 2011). s_c was obtained from REMA with typical elevation errors of less than 1 m (Howat et
205 al., 2019). Firn depth correction and its uncertainty were calculated from regional climate model RACMO2/ANT with a ratio accounting for 8% (Pritchard et al., 2012).

https://doi.org/10.5194/essd-2020-340
Preprint. Discussion started: 15 January 2021

c) Calving mass uncertainty. The calving mass of our dataset is derived from three components unrelated to and independent of each other. Thus, we used synthetic standard uncertainty to evaluate its accuracy. The mass deviation of a single calving event (U_c) is as follows Eq. (5), and the mass deviation for the year cycle ($\overline{U_C}$) can be calculated from Eq. (6):

$$U_c = C \times \sqrt{\frac{U_A^2}{A_c^2} + \frac{U_{\overline{H}}^2}{\overline{H}^2} + \frac{U_{\rho_{ice}}^2}{\rho_{ice}^2}}, \quad (5)$$

$$\overline{U_C} = \frac{\sqrt{\sum_{i=1}^{n} U_{C_i}^2}}{N}, \quad (6)$$

where C and A_c are the mass and area of individual calving events, respectively. N is the number of years, and n is the total frequency of calving events that occurred in N years.

3.3.3 Recurrence interval and its classification

The recurrence interval is defined as the year interval between two independent calving events at the same calving front. Calving recurrence happens when two calving events occur in the same spatial neighbourhood, and their areas are of the same order of magnitude (Liu et al., 2015). To acquire this attribute, we performed the following work. First, we converted the calved-area polygons to their centre points, assigned different buffer radii to calving events at different scales and built buffers for each calving point. With our product, we designed the buffer radius as one-half the average perimeter of all calving events at the same scale for 14 years and then rounded up to the nearest integer. The specific values used for the product are shown in Table 3.

Table 3: Parameters used to define the calving recurrence interval.

Size	Perimeter (range)/km	Perimeter (average)/km	Buffer radius/km
Small-scale (< 10 km^2)	[4.0, 45.3]	11.8	6
Medium-scale (10-100 km^2)	[14.4, 136.2]	37.4	19
Large-scale (100-1000 km^2)	[45.4, 184.0]	93.6	47
Extra-large-scale (>1000 km^2)	[182.5, 479.5]	310.2	155

We calculated the number of points for the same scale and year falling within the buffer of each calving event. For buffers with more than three points, the calving recurrence interval was defined as the total number of years (14) divided by the exact number of points falling within. For buffers with two points, the calving recurrence interval was defined as the gap between the two calving points. For buffers with only one point, also defined as central buffer points, the calving recurrence interval was defined as the greater value of its distance to the boundary years (2005 or 2019).

According to the calving recurrence interval, we classified the annual iceberg calving events into two different types: high-frequency (calving recurrence interval of ⩽7 years) and low-frequency calving events (calving recurrence interval of >7 years). The longer the recurrence interval is, the less calving that occurs in a given period and the lower the frequency.

https://doi.org/10.5194/essd-2020-340
Preprint. Discussion started: 15 January 2021

3.4 Consistency validation of multisource satellite imagery

As mentioned above, a single satellite platform cannot accommodate long time series observations of circum-Antarctic calving events. Thus, multisource remotely sensed data are used in this study. To check whether the results derived from different sensors are similar, especially for the results derived from optical sensors and SAR, we performed the following verification.

For the year for which we have both SAR and optical images, we extracted circum-Antarctic annual iceberg calving using the same method based on different sources of remotely sensed imagery. We chose to repeat the calving extraction for 2016/17 through Terra/Aqua MODIS imagery and to compare it to the contemporaneous extraction results for our dataset derived from Sentinel-1 SAR imagery. We define area differences as the calving area obtained from MODIS subtracted from that obtained from SAR, and we define the calving perimeter as the calved-area perimeter obtained from SAR. Then, we analyse the area differences of the same calving events and calculate error-equivalent perimeter widths by dividing the area differences by the calving perimeter.

4. Validation and Uncertainty

4.1 Consistency of multi-source satellite imagery

We extracted a total of 220 calving events from MODIS for 2016/17 covering a total area of 9064.6 km^2. As shown in Table 4, both the total calving frequency and total calving area are slightly lower than those derived from SAR imagery. The calving frequencies at different scales extracted from the two sources of satellite images are similar. The calving frequency error mainly originates from small-scale calving, although it accounts for a small percentage of the total area. The calving area derived from MODIS at all four scales is underestimated compared with that from SAR, which might be a result of lower image quality for cloudy areas.

Table 4: Frequency and area distribution of different scale calving events derived from MODIS and SAR for 2016/17

	Scale	MODIS	SAR	Δ(MODIS-SAR)	Δ(MODIS-SAR)/SAR$_{Total}$
Calving frequency	Small-scale	163	167	-4	-1.8%
	Medium-scale	50	50	1	0.4%
	Large-scale	6	6	0	-
	Extra-large-scale	1	1	0	-
	Total	220	224	-4	-1.8%
Calving area (km^2)	Small-scale	511.0	563.0	-52.0	-0.6%
	Medium-scale	1441.0	1478.2	-37.2	-0.4%
	Large-scale	1057.9	1077.9	-20.0	-0.2%
	Extra-large-scale	6054.7	6141.0	-86.3	-0.9%
	Total	9064.6	9260.2	-195.5	-2.1%

The area of individual calving events extracted by MODIS is generally smaller. As the calving scale increases, errors caused by different data sources account for a lower percentage of the calving area (Figure 4 (a)(b)(c)). The error-equivalent perimeter widths generally exhibit a normal distribution with a standard deviation of 0.15 km and a mean value of -0.06 km (Figure 4 (d)). Based on this, the errors introduced by multisource satellite data are acceptable.

https://doi.org/10.5194/essd-2020-340
Preprint. Discussion started: 15 January 2021

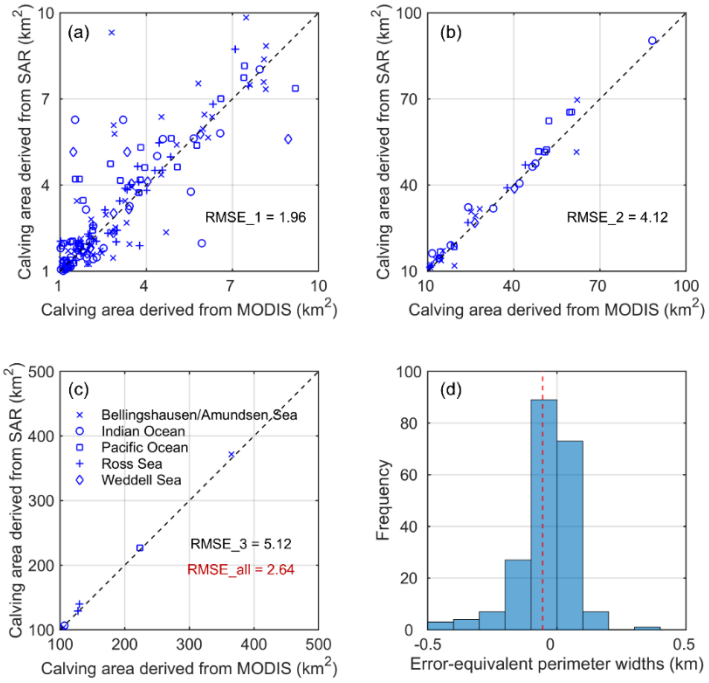

Figure 4: Comparison of areas of individual calving extracted from MODIS and SAR for 2016/17. Panels (a), (b), and (c) show the small-scale, medium-scale, and large-scale calving events, respectively. Panel (d) shows the error distribution histogram of error-equivalent perimeter widths.

4.2 Attribute uncertainties

We assessed the accuracy of calving area, calved-area thickness, and calving mass attributes with Eq. (2), (4), (5), and (6).

The maximum area measurement uncertainty of a single calving event represented in this dataset was calculated as 30.7 km^2 with an annual average calving area uncertainty value of 17.1 km^2. Thickness uncertainty is mainly attributed to firn depth correction. For individual calving events, thickness uncertainty ranges from 1.0 m to 67.7 m with a mean value of 18.5 m. Calving mass uncertainty is mainly determined by thickness uncertainty with a mean value of 10.2 Gt for 14 years, and its annual percentage fluctuates from 1.9% to 6.0% each year.

5. Temporal and spatial variations in Antarctic iceberg calving

5.1 Calving frequency, area and mass

Using the newly developed dataset, we identify 1786 annual calving events covering areas of larger than 1 km^2 occurring in the circum-Antarctic ice shelf from August 2005 to August 2019. The average annual calving frequency, area and mass are 127.6 times, 3411.4 km², and 771.1 Gt, respectively. The calving frequency, area and mass show high levels of year-to-year variability (Table 4), highlighting the need for longer records to determine long-term changes in ice shelves.

https://doi.org/10.5194/essd-2020-340
Preprint. Discussion started: 15 January 2021

The calving frequency seems to be stable for the period of 2005/06-2015/16, fluctuating from 69 to 127, but it increases substantially in 2015/16 and fluctuates from 168 to 225 for the period of 2015/16-2018/19. The total calving area is anomalously low in 2006/07 compared to other years. Then, it increases in the following three years and especially in 2008/09 and 2009/10, during which two extra-large calving events occurred in the Wilkins Ice Shelf and Mertz Ice Shelf. Then, the calving area decreased again in 2010/11 and fluctuated in 2010/11-2014/15. In 2016/17, the calving area increased considerably to a maximum of 9262.0 km^2 over the 14 years, during which an extra-large disintegration of the Larsen C Ice Shelf occurred. After that, we find the most dramatic reduction in 2017/18, with a total calving area of 1386.3 km^2 reducing to a minimum during the observation cycle. In 2018/19, the calving area rose slightly to a level close to that of 2005/06-2015/16. For annual calving mass, the maximum value appeared in 2016/17 at 1832.6 Gt, and the minimum value in 2010/11 was recorded at 332.0 Gt. This fluctuating trend of calving mass is generally consistent with that of the calving area.

Table 5: Annual distribution of cumulative iceberg calving frequency, area, and mass for August 2005 to August 2019.

Year	Calving frequency	Calving area/ km^2	Calving mass/ Gt
2005/06	127	3372.5	755.9
2006/07	98	1702.5	402.0
2007/08	69	2775.3	570.8
2008/09	113	4341.3	704.4
2009/10	87	4261.5	1001.7
2010/11	83	1707.6	332.0
2011/12	95	3218.3	847.4
2012/13	119	2932.2	762.7
2013/14	99	2148.0	562.3
2014/15	73	2262.4	552.5
2015/16	206	5584.5	1398.8
2016/17	224	9260.2	1832.6
2017/18	168	1386.3	338.9
2018/19	225	2806.4	732.9
Average	127.6	3411.4	771.1
Total	1786	47759.0	10795.0

5.2 Calving scale

The annual distributions of calving frequency, area, and mass at different scales are shown in panels (a), (c), and (e) of Figure 5. Over the 14 years, the cumulative calving frequencies of small-, medium-, large- and extra-large-scale events accounted for 71.9%, 24.3%, 3.5%, and 0.3%, respectively, and frequencies increased exponentially as the scale decreased. The cumulative calving areas of the four different sizes accounted for 9.4%, 26.1%, 31.7%, and 32.8%, respectively. The distribution of calving mass is similar to that of the calving area.

The frequency of small-scale calving accounts for a large percentage of total calving, especially in 2015/16-2018/19. The interannual variations in small-scale calving frequency show obviously moderate variations. However, the area and mass of small-scale calving remain relatively stable and low. As the calving scale increases, interannual variations in frequency become less significant; in contrast, interannual variations in area and mass become increasingly volatile. In some years, calving

https://doi.org/10.5194/essd-2020-340
Preprint. Discussion started: 15 January 2021

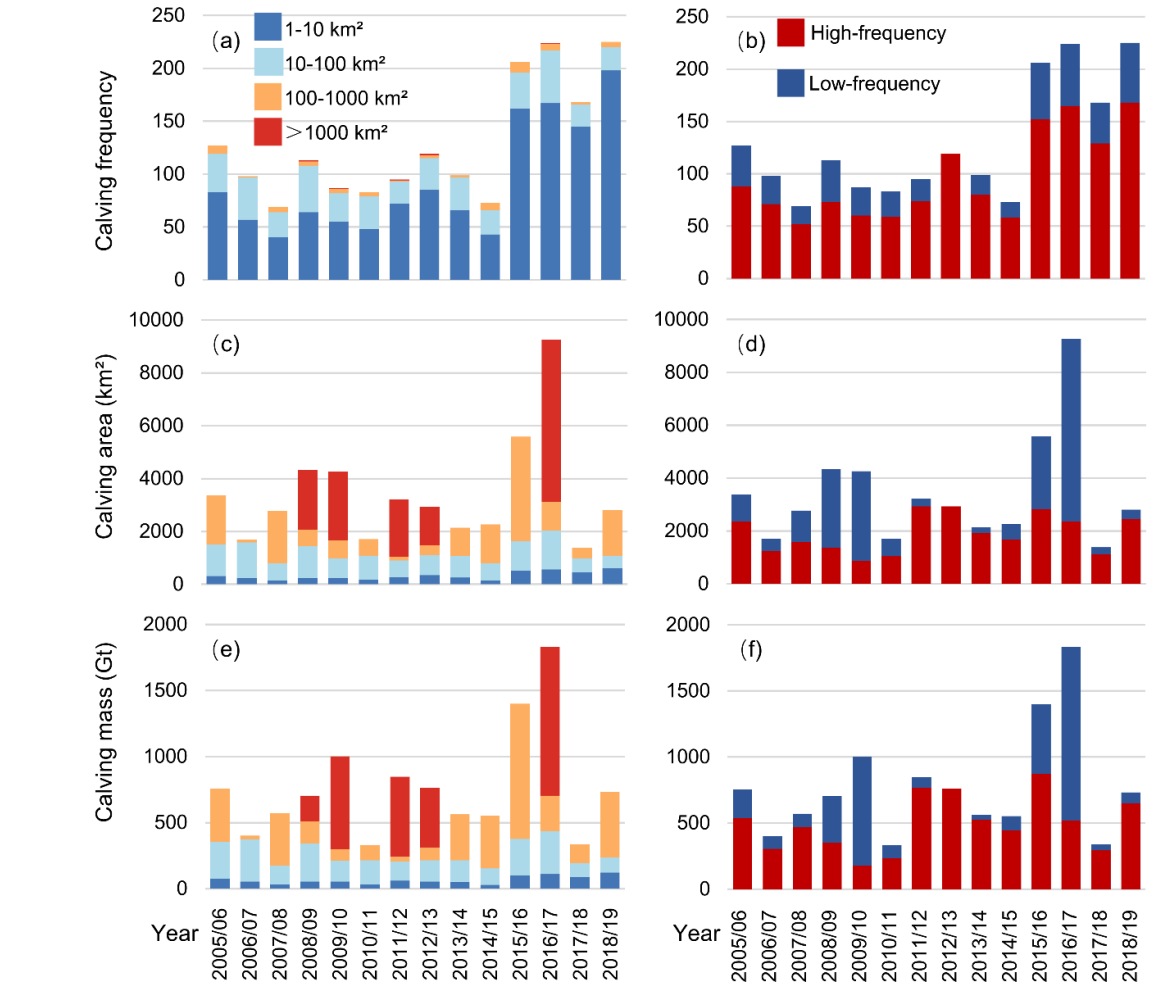

Figure 5: Cumulative distribution of annual calving events for different scales and types of Antarctic ice shelves for August 2005 to August 2019. Panels (a), (c), and (e) present the annual calving frequency, area, and mass at four scales, respectively. Panels (b), (d), and (f) illustrate the three indicators for the two calving types.

5.3 Calving recurrence interval and calving type

The cumulative frequency, area, and mass distribution under different calving recurrence intervals are shown in Figure 6. These three indicators show an approximate double-peak distribution. Calving events with a recurrence interval of 3 had the highest frequency, accounting for 18.8% of the total and occurring 335 times in 14 years, followed by those with recurrence intervals of 5, 2 and 4, accounting for 18.5%, 15.2% and 14.3%, respectively. With the increase in recurrence interval values,

https://doi.org/10.5194/essd-2020-340
Preprint. Discussion started: 15 January 2021

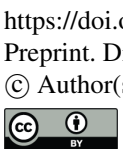

the frequency, area, and mass first increased to a peak, and then the overall trend was downward; thereafter, calving frequency reached another insignificant peak while both area and mass grew to a new peak with a similar magnitude to the first one.

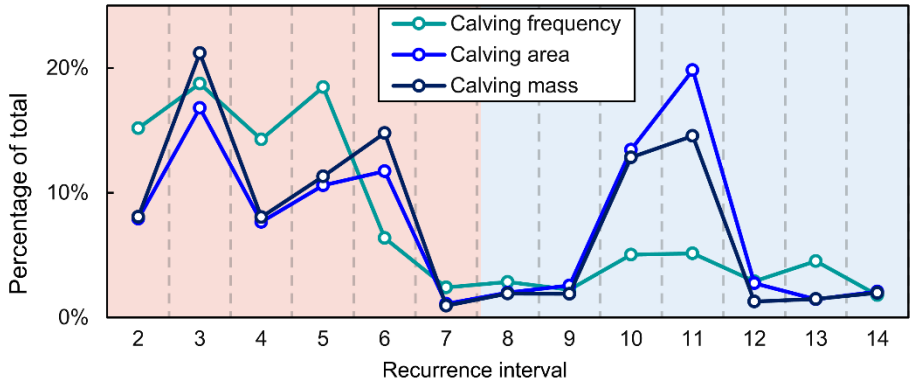

Figure 6: The proportional distribution of calving frequency, area, and mass for different recurrence intervals of calving events.

Time series of the annual different-type cumulative distributions of calving frequency, area, and mass are shown in Figure 5 (b), (d), and (f), respectively. Trends in the frequency of low- and high-frequency calving are similar, but there is a large difference in the interannual distributions of the area and mass of the two types of calving.

For high-frequency calving, its interannual variation is more consistent with the total frequency. For low-frequency calving, the interannual trend is more consistent with the total calving area and mass, which fluctuates more than that of low-frequency calving.

5.4 Spatial distribution of annual calving events

Figure 7 shows the spatial distribution of annual calving events of different scales and types for 2005/06 to 2018/19. Small- and medium-scale calving widely appeared in the Antarctic Peninsula, in West Antarctica, and on Wilkes Land in East Antarctica with interannual variations mainly found in Queen Maud Land in East Antarctica from 2011/12-2015/16. In 2011/12-2015/16, small-scale calving events were largely distributed in West Antarctica and sparsely occurred in East Antarctica. Large-scale calving events appeared quite randomly, usually in medium-sized ice shelf regions of the Antarctica Peninsula and of West Antarctica. Extra-large-scale calving events occurred only twice in the Antarctica Peninsula, twice in West Antarctica, and once in East Antarctica.

High-frequency calving is most common on small ice shelves in West Antarctica, followed by the Antarctica Peninsula and Wilkes Land in East Antarctica. Low-frequency calving shows considerable variation in the interannual distribution, especially for Queen Maud Land and Wilkes Land, which present an obscure spatial pattern.

https://doi.org/10.5194/essd-2020-340
Preprint. Discussion started: 15 January 2021

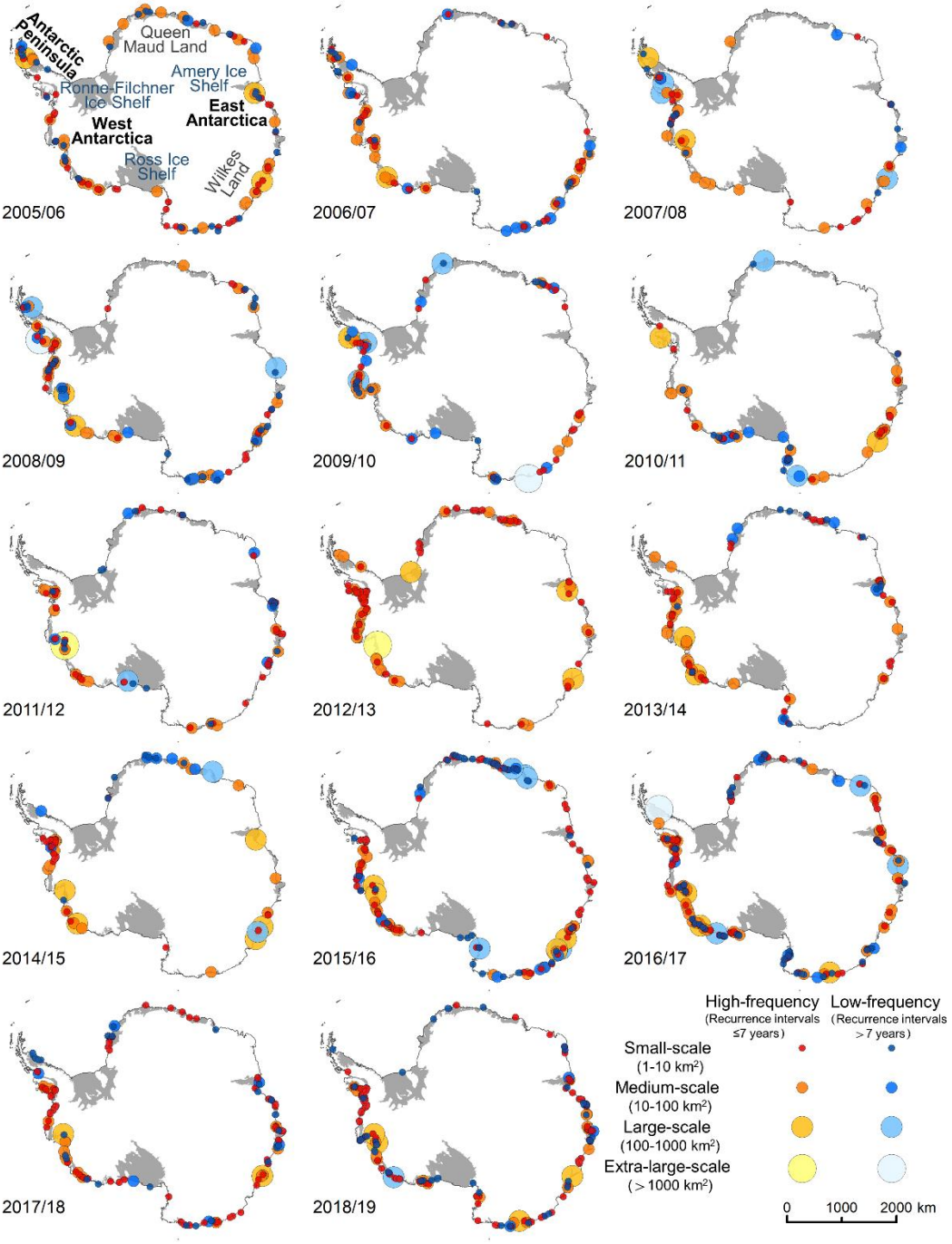

Figure 7: Spatial distribution of annual calving events for different scales and types of Antarctic ice shelves for August 2005 to August 2019.

Figure 8 shows the annual average calving mass distribution of Antarctic ice shelves. We find that the calving mass of Antarctica is mainly affected by the iceberg calving of small ice shelves rather than that of larger ice shelves. Of these, the

https://doi.org/10.5194/essd-2020-340
Preprint. Discussion started: 15 January 2021

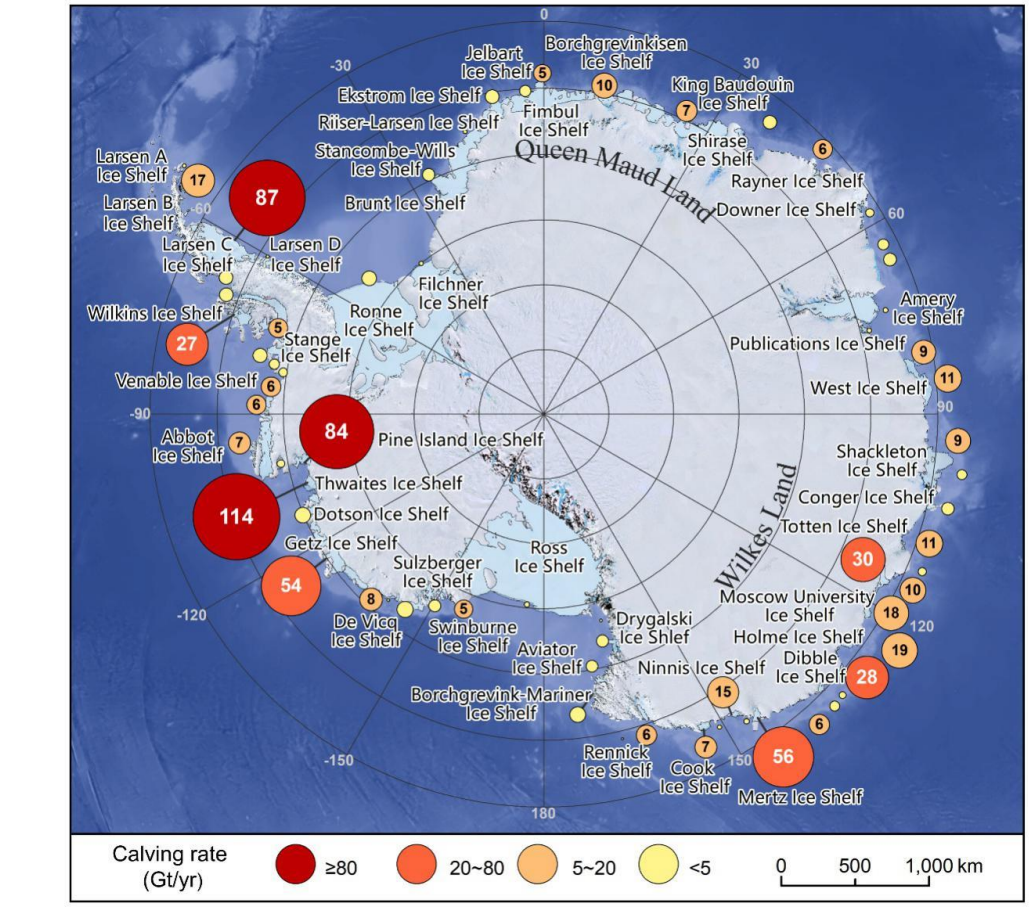

Figure 8: Average calving rate (Gt/yr) of Antarctic ice shelves for 2005-2019.

https://doi.org/10.5194/essd-2020-340
Preprint. Discussion started: 15 January 2021

6. Discussion and conclusion

In this study, we developed a 14-year circum-Antarctic iceberg calving dataset using continuous multisource optical and SAR images for August 2005 to August 2019. Independent annual calving events covering areas larger than 1 km^2 were obtained through velocity-based ice shelf front edge simulation and semiautomatic extraction (Qi et al., 2020). Furthermore, we acquired the year, area, thickness, mass, recurrence interval and type of calving and calculated the uncertainties of the results. The accuracy assessment shows an average level of annual calving area uncertainty of ±17.1 km^2, an average thickness uncertainty of all calving events of ±18.5 m, and an average annual calving mass uncertainty value of ±10.2 Gt. A preliminary analysis of temporal and spatial characteristics of Antarctic iceberg calving events of the last 14 years was then conducted. In total, 1786 annual calving events covering areas larger than 1 km^2 occurred in the circum-Antarctic ice shelf from August 2005 to August 2019. The average annual calving frequency, area, and mass were recorded as 127.6 times, 3411.4 km^2, and 771.1 Gt, respectively. Spatially, the West Antarctic is more active in terms of calving than the East Antarctic, and the small ice shelves are more active than the large ice shelves. Temporally, the calving frequency, area, and mass remained relatively stable from 2005/06 to 2014/15 and increased to a higher level from 2015/16 to 2016/17. After that, the calving frequency was still high in 2017/18-2018/19, but the calving area and mass decreased to their lowest values in the 14 years.

This new dataset provides an opportunity to examine the potential associations between iceberg calving and remote and local climate forcings. Here, we show two examples from our preliminary analysis. First, Figure 9 (c) and (a) shows the relationship between calving indicators (frequency, area, and mass) and the oceanic Niño index. Remotely, El Niño leads to anomalous increases in sea surface temperature and Antarctic ice sheet temperature. We found that a strong El Niño might lead to an increase in the calving frequency, area and mass of Antarctic ice shelves, and there has been intensified iceberg calving since then.

Second, Figure 9 (c) and (b) shows the correlation between iceberg calving and ice sheet surface melting. Locally, atmospheric warming intensified ice sheet surface melting, resulting in increased meltwater, which may trigger the expansion of rifts and crevasses and finally enhance iceberg calving. Based on this dataset, we found significantly positive correlations between the maximum daily surface melting area and calving frequency ($r=0.76$, $p=0.003$), calving area ($r=0.75$, $p=0.002$), and calving mass ($r=0.65$, $p=0.0172$).

https://doi.org/10.5194/essd-2020-340
Preprint. Discussion started: 15 January 2021

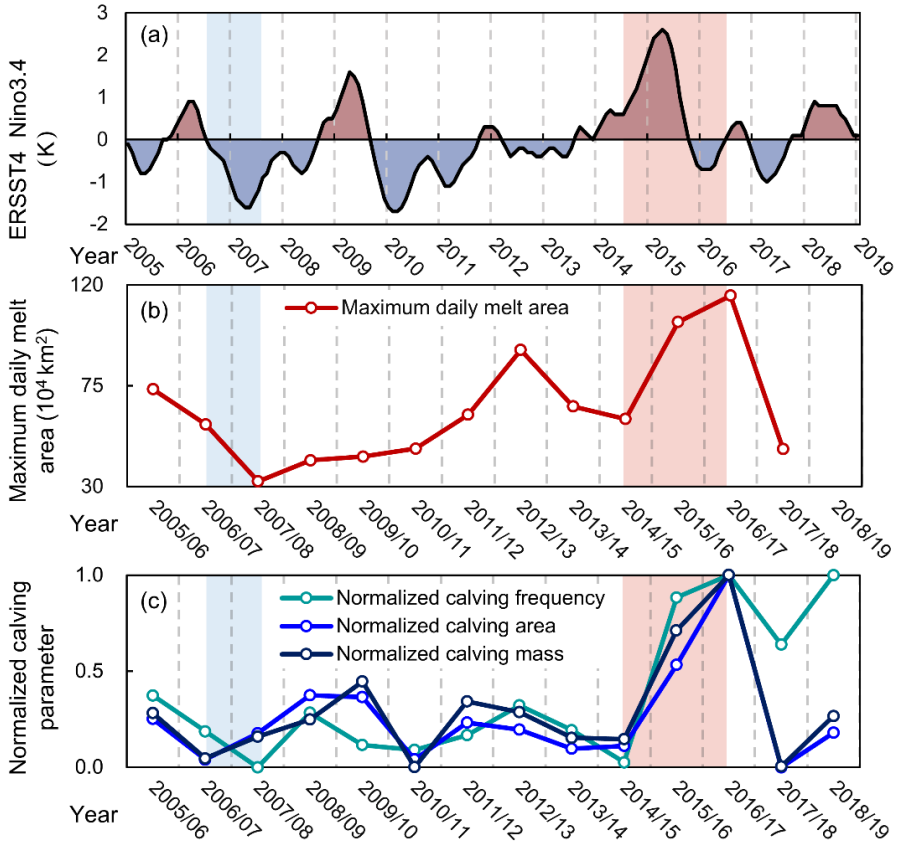

Figure 9: Relationship between annual iceberg calving distribution for 2005 to 2019 and (a) oceanic Niño index data from https://ggweather.com/enso/oni.htm and (b) maximum daily ice sheet surface melting area data from http://pp.ige-grenoble.fr/pageperso/picardgh/melting/

In summary, the annual circum-Antarctic iceberg calving dataset (2005-2019) is the first to provide consistent and precise calving observations with the longest time span of 15 years. It not only directly reflects the quantitative characteristics and spatial distribution of Antarctic iceberg calving but also provides multidimensional variables of each independent calving event. This dataset can be used as fundamental data for subsequent studies on ice sheet mass balance, calving mechanisms, and their responses to climate change.

7. Data availability

The developed iceberg calving product applies a 14-year calving distribution with year, length, area, size, thickness, mass, recurrence interval, type and measurement uncertainty attributes for each calving event. The product applies an annual temporal resolution, and its spatial resolution is set to 1 km². The dataset is stored in Shapefile format, shared via the Global Change Data Repository (http://www.geodoi.ac.cn), and titled "Annual iceberg calving dataset of the Antarctic ice shelves (2005-2019)" with DOI: 10.3974/geodb.2020.04.09.V1 (Qi et al., 2020a).

Author Contributions. X.C, Y.L and M.Q. conceived of, designed and conducted the experiment. Y.L and M.Q. contributed to the research framework and helped develop the methodology. M.Q and Y.L. performed the data analysis. M.Q, Y.L, J.L, and Q.S. contributed to analysing the results. M.Q and Q.F. contributed to the data processing. All authors contributed to the discussion and writing of the manuscript.

Competing interests. The authors declare that they have no conflict of interest.

Acknowledgments. We greatly thank European Space Agency (ESA) for providing the Sentinel-1 and Envisat imagery, we thank the National Aeronautics and Space Administration (NASA) and United States Geological Survey (USGS) for providing the Landsat and MODIS data, and we truly appreciate the National Snow and Ice Data Center (NSIDC) for providing the ice velocity and ice-sheet boundary products. We thank British Antarctic Survey (BAS) for providing the Bedmap 2 and Polar Geospatial Center at University of Minnesota and UGA for providing the Reference Elevation Model for Antarctica（REMA).

Financial support. This research was funded by the National key research and development Program of China (Grant No. 2016YFA0600103 and Grant No. 2018YFA0605403), National Natural Science Foundation of China (Grant No. 41925027), and Qian Xuesen Lab. - DFH Sat. Co. Joint Research and Development Fund.

References

Åström, J. A., Vallot, D., Schäfer, M., Welty, E. Z., O'Neel, S., Bartholomaus, T. C., Liu, Y., Riikilä, T. I., Zwinger, T., Timonen, J., and Moore, J. C.: Termini of calving glaciers as self-organized critical systems, Nature Geoscience, 7, 874-878, 10.1038/ngeo2290, 2014.

Berthier, E., Scambos, T. A., and Shuman, C. A.: Mass Loss of Larsen B Tributary Glaciers (Antarctic Peninsula) Unabated Since 2002, Geophys. Res. Lett., 39, 2012.

Bindschadler, R.: History of lower Pine Island Glacier, West Antarctica, from Landsat imagery, J. Glaciol., 48, 536-544, 2002.

Cook, A. J., Fox, A. J., Vaughan, D. G., and Ferrigno, J. G.: Retreating glacier fronts on the Antarctic Peninsula over the past half-century, science, 308, 541-544, 10.1126/science.1104235, 2005.

Cook, A. J., and Vaughan, D. G.: Overview of areal changes of the ice shelves on the Antarctic Peninsula over the past 50 years, Cryosphere, 4, 77-98, 10.5194/tc-4-77-2010, 2010.

Depoorter, M. A., Bamber, J. L., Griggs, J. A., Lenaerts, J. T., Ligtenberg, S. R., van den Broeke, M. R., and Moholdt, G.: Calving fluxes and basal melt rates of Antarctic ice shelves, Nature, 502, 89-92, 10.1038/nature12567, 2013.

Fountain, A. G., Glenn, B., and Scambos, T. A.: The Changing Extent of the Glaciers Along the Western Ross Sea, Antarctica, Geology, 45, 927-930, 2017.

Fretwell, P., Pritchard, H. D., Vaughan, D. G., Bamber, J. L., Barrand, N. E., Bell, R., Bianchi, C., Bingham, R. G., Blankenship, D. D., Casassa, G., Catania, G., Callens, D., Conway, H., Cook, A. J., Corr, H. F. J., Damaske, D., Damm, V., Ferraccioli, F., Forsberg, R., Fujita, S., Gogineni, P., Griggs, J. A., Hindmarsh, R. C. A., Holmlund, P., Holt, J. W., Jacobel, R. W., Jenkins, A., Jokat, W., Jordan, T., King, E. C., Kohler, J., Krabill, W., Riger-Kusk, M., Langley, K. A., Leitchenkov, G., Leuschen, C., Luyendyk, B. P., Matsuoka, K., Nogi, Y., Nost, O. A., Popov, S. V., Rignot, E., Rippin, D. M., Riviera, A., Roberts, J., Ross, N., Siegert, M. J., Smith, A. M.,

https://doi.org/10.5194/essd-2020-340
Preprint. Discussion started: 15 January 2021

Steinhage, D., Studinger, M., Sun, B., Tinto, B. K., Welch, B. C., Young, D. A., Xiangbin, C., and Zirizzotti, A.: Bedmap2: improved ice bed, surface and thickness datasets for Antarctica, The Cryosphere Discussions, 6, 4305-4361, 10.5194/tcd-6-4305-2012, 2012.

Furst, J. J., Durand, G., Gilletchaulet, F., Tavard, L., Rankl, M., Braun, M., and Gagliardini, O.: The safety band of Antarctic ice shelves, Nat. Clim. Chang., 6, 479-482, 2016.

Griggs, J. A., Bamber, and L, J.: Antarctic ice-shelf thickness from satellite radar altimetry, J. Glaciol., 57, 485-498, 2011.

Hill, E. A., Carr, J. R., Stokes, C. R., and Gudmundsson, G. H.: Dynamic changes in outlet glaciers in northern Greenland from 1948 to 2015, Cryosphere, 12, 3243-3263, 2018.

Howat, I. M., Porter, C., Smith, B., Noh, M. J., and Morin, P.: The Reference Elevation Model of Antarctica, Cryosphere, 13, 665-674, 2019.

Liu, H., and Jezek, K. C.: A Complete High-Resolution Coastline of Antarctica Extracted from Orthorectified Radarsat SAR Imagery, Photogrammetric Engineering Remote Sensing, 70, 605-616, 2004.

Liu, Y., Cheng, X., Hui, F., Wang, F., and Chi, Z.: Antarctic iceberg calving monitoring based on EnviSat ASAR images, Journal of Remote Sensing, 17, 479-494, 2013.

Liu, Y., Moore, J. C., Cheng, X., Gladstone, R. M., Bassis, J. N., Liu, H., Wen, J., and Hui, F.: Ocean-driven thinning enhances iceberg calving and retreat of Antarctic ice shelves, Proceedings of the National Academy of Sciences of the United States of America, 112, 3263-3268, 10.1073/pnas.1415137112, 2015.

Lovell, A. M., Stokes, C. R., and Jamieson, S. S. R.: Sub-decadal variations in outlet glacier terminus positions in Victoria Land, Oates Land and George V Land, East Antarctica (1972–2013), Antarctic Science, 29, 468-483, 2017.

Luckman, A., Benn, D. I., Cottier, F., Bevan, S., Nilsen, F., and Inall, M.: Calving rates at tidewater glaciers vary strongly with ocean temperature, Nature Communications, 6, 8566-8566, 2015.

Massom, R. A., Giles, A. B., Warner, R. C., Fricker, H. A., Legresy, B., Hyland, G., Lescarmontier, L., and Young, N. W.: External influences on the Mertz Glacier Tongue (East Antarctica) in the decade leading up to its calving in 2010, J. Geophys. Res., 120, 490-506, 2015.

Massom, R. A., Scambos, T. A., Bennetts, L. G., Reid, P., Squire, V. A., and Stammerjohn, S. E.: Antarctic ice shelf disintegration triggered by sea ice loss and ocean swell, Nature, 558, 383-389, 10.1038/s41586-018-0212-1, 2018.

MCST: MODIS 250m Calibrated Radiances Product, http://dx.doi.org/10.5067/MODIS/MOD02QKM.061, 2017.

Medrzycka, D., Benn, D. I., Box, J. E., Copland, L., and Balog, J.: Calving Behavior at Rink Isbræ, West Greenland, from Time-Lapse Photos, Arct. Antarct. Alp. Res., 48, 263-277, 10.1657/aaar0015-059, 2016.

Miles, B. W. J., Stokes, C. R., and Jamieson, S. S. R.: Simultaneous disintegration of outlet glaciers in Porpoise Bay (Wilkes Land), East Antarctica, driven by sea ice break-up, Cryosphere, 11, 427-442, 2017.

Morlighem, M., Rignot, E., Binder, T., Blankenship, D. D., Drews, R., Eagles, G., Eisen, O., Ferraccioli, F., Forsberg, R., and Fretwell, P. T. J. N. G.: Deep glacial troughs and stabilizing ridges unveiled beneath the margins of the Antarctic ice sheet, Nat. Geosci., 13, 132-137, 2020.

Mouginot, J., Scheuchl, B., and Rignot, E.: Mapping of Ice Motion in Antarctica Using Synthetic-Aperture Radar Data, Remote Sens., 4, 2753-2767, 10.3390/rs4092753, 2012.

Mouginot, J., Rignot, E., Scheuchl, B., and Millan, R.: Comprehensive Annual Ice Sheet Velocity Mapping Using Landsat-8, Sentinel-1, and RADARSAT-2 Data, Remote Sens., 9, 10.3390/rs9040364, 2017.

Pattyn, F., and Morlighem, M.: The uncertain future of the Antarctic Ice Sheet, science, 367, 1331-1335, 10.1126/science.aaz5487, 2020.

Picard, G., and Fily, M.: Surface melting observations in Antarctica by microwave radiometers: Correcting 26-year time series from changes in acquisition hours, Remote Sensing of Environment, 104, 325-336, 2006.

Pritchard, H. D., Ligtenberg, S. R. M., Fricker, H. A., Vaughan, D. G., van den Broeke, M. R., and Padman, L.: Antarctic ice-sheet loss driven by basal melting of ice shelves, Nature, 484, 502-505, 10.1038/nature10968, 2012.

Qi, M., Liu, Y., Cheng, X., Feng, Q., Hui, F., and Chen, Z.: Annual Iceberg Calving Dataset of the Antarctic Ice Shelves (2005-2019), Global Change Data Repository, 10.3974/geodb.2020.04.09.V1, 2020a.

https://doi.org/10.5194/essd-2020-340
Preprint. Discussion started: 15 January 2021

Qi, M., Liu, Y., Lin, Y., Hui, F., Li, T., and Cheng, X.: Efficient Location and Extraction of the Iceberg Calved Areas of the Antarctic Ice Shelves, Remote Sensing, 12, 10.3390/rs12162658, 2020b.

Rignot, E., Casassa, G., Gogineni, P., Krabill, W. B., Rivera, A., and Thomas, R.: Accelerated Ice Discharge from the Antarctic Peninsula following the Collapse of Larsen B Ice Shelf, Geophys. Res. Lett., 31, 1-4, 2004.

Rignot, E., Mouginot, J., and Scheuchl, B.: Ice flow of the Antarctic ice sheet, science, 333, 1427-1430, 10.1126/science.1208336, 2011.

Rignot, E., Jacobs, S., Mouginot, J., and Scheuchl, B.: Ice-shelf melting around Antarctica, Science, 341, 266-270, 10.1126/science.1235798, 2013a.

Rignot, E., Jacobs, S. S., Mouginot, J., and Scheuchl, B.: Ice-Shelf Melting Around Antarctica, Science, 341, 266-270, 10.1126/science.1235798, 2013b.

Rignot, E., Mouginot, J., and Scheuchl, B.: MEaSUREs InSAR-Based Antarctica Ice Velocity Map, Version 2, Boulder, Colorado USA. NASA National Snow and Ice Data Center Distributed Active Archive Center. , https://doi.org/10.5067/D7GK8F5J8M8R., 2017.

Scambos, T. A., Haran, T., Fahnestock, M., Painter, T. H., and Bohlander, J.: MODIS-based Mosaic of Antarctica (MOA) data sets: Continent-wide surface morphology and snow grain size, Remote Sensing of Environment, 111, 242-257, 2007.

Yu, Y., Zhang, Z., Shokr, M., Hui, F., Cheng, X., Chi, Z., Heil, P., and Chen, Z.: Automatically Extracted Antarctic Coastline Using Remotely-Sensed Data: An Update, Remote Sens., 11, 10.3390/rs11161844, 2019.

Zhao, C., Cheng, X., Hui, F., Kang, J., Liu, Y., Wang, X., Wang, F., Cheng, C., Feng, Z., Ci, T., Zhao, T., and Zhai, M.: Monitoring the Amery Ice Shelf front during 2004-2012 using ENVISAT ASAR data, Advances in Polar Science, 24, 133-137, 10.3724/sp.J.1085.2013.00133, 2014.